Multifunctional Poly(2,5-benzimidazole)/Carbon Nanotube Composite Films

JI-YE KANG,[1] SOO-MI EO,[1] IN-YUP JEON,[1] YEONG SUK CHOI,[2] LOON-SENG TAN,[3] JONG-BEOM BAEK[1]

[1]School of Energy Engineering, Ulsan National Institute of Science and Technology (UNIST), 194, Banyeon, Ulsan 689-805, South Korea

[2]Energy and Environment Laboratory, Samsung Advanced Institute of Technology, Suwon 449-600, South Korea

[3]Nanostructured and Biological Materials Branch, Materials and Manufacturing Directorate, Air Force Research Laboratory, AFRL/RXBN, Wright-Patterson Air Force Base, Dayton, Ohio 45433-7750

Received 27 October 2009; accepted 28 November 2009
DOI: 10.1002/pola.23862
Published online in Wiley InterScience (www.interscience.wiley.com).

ABSTRACT: The AB-monomer, 3,4-diaminobenzoic acid dihydrochloride, was recrystallized from an aqueous hydrochloric acid solution and used to synthesize high-molecular-weight poly(2,5-benzimidazole) (ABPBI). ABPBI/carbon nanotube (CNT) composites were prepared via *in situ* polymerization of the AB-monomer in the presence of single-walled carbon nanotube (SWCNT) or multiwalled carbon nanotube (MWCNT) in a mildly acidic polyphosphoric acid. The ABPBI/SWCNT and ABPBI/MWCNT composites displayed good solubility in methanesulfonic acid and thus, uniform films could be cast. The morphology of these composite films was studied by X-ray diffraction, scanning electron microscopy, transmission electron microscopy, and atomic force microscopy. The results showed that both types of CNTs were uniformly dispersed into the ABPBI matrix. Tensile properties of the composite films were significantly improved when compared with ABPBI, and their toughness (~200 MPa) was close to the nature's toughest spider silk (~215 MPa). The electrical conductivities of ABPBI/SWCNT and ABPBI/MWCNT composite films were 9.10×10^{-5} and 2.53×10^{-1} S/cm, respectively, whereas that of ABPBI film was 4.81×10^{-6} S/cm. These values are ~19 and 52,700 times enhanced by the presence of SWCNT and MWCNT, respectively. Finally, without acid impregnation, the ABPBI film was nonconducting while the SWCNT- and MWCNT-based composites were proton conducting with maximum conductivities of 0.018 and 0.017 S/cm, respectively. © 2010 Wiley Periodicals, Inc. J Polym Sci Part A: Polym Chem 48: 1067–1078, 2010

KEYWORDS: composites; high-performance polymers; *in situ* polymerization; multiwalled carbon nanotube (MWCNT); nanocomposites; poly(2,5-benzimidazole); (ABPBI); polycondensation; poly(phosphoric acid); single-walled carbon nanotube (SWCNT); toughness

INTRODUCTION Polymer–matrix composites have been studied for 5 decades as a special class of high-performance, lightweight materials that continue to play important roles in the current and emerging technologies for application areas ranging from structural, electronic, electromagnetic-shielding, to smart materials.[1] Typically, they are prepared by dispersing rigid and strong fibers such as glass and carbon fibers in a polymer matrix, and their resulting properties (primarily because of the surface area and aspect ratio limitations associated with the reinforcement additive) are greatly dependent on the loading amount of a particular filler, which generally requires a significant quantity (~60 vol %).[1] On the other hand, nanoscale additives, such as nanoclays,[2] nanoparticles,[3] nanoplatelets,[4] and carbon nanotubes (CNTs),[5] can overcome such limitations, and when dispersed in a polymer matrix, they could dramatically change the properties of resultant composite at lower loadings. Among them, CNTs such as single-walled carbon nanotubes (SWCNTs) and multiwalled carbon nanotube (MWCNTs) have attracted considerable attention because of expected excellent mechanical, thermal, and electrical properties attributed to their unique structures that are also amenable to a wide range of chemical modification.[6] They could be used as reinforcing additives and thus deliver their outstanding properties to the supporting matrices.[7] The resultant composites could be used in application areas, where affordable, lightweight, and multifunctional materials are required. To take advantage of their mechanical properties as predicted, several studies have been performed on CNTs and reported their reinforcement in various thermoplastics and thermoset matrices.[8] However, there are two major obstacles for polymer/CNT composites to achieve maximum level of enhanced composite properties. First, it is nontrivial to achieve the effective aspect ratio by homogeneous dispersion of CNT in polymer matrix.[9] This is followed by the necessity to (i) efficiently transfer the outstanding properties of CNT to the supporting matrix and (ii) form effective percolation network at low loading. Hitherto, many efforts have been devoted to

Additional Supporting Information may be found in the online version of this article. Correspondence to: J.-B. Baek (E-mail: jbbaek@unist.ac.kr)
Journal of Polymer Science: Part A: Polymer Chemistry, Vol. 48, 1067–1078 (2010)

Report Documentation Page

Form Approved
OMB No. 0704-0188

1. REPORT DATE	2. REPORT TYPE	3. DATES COVERED
2010		**00-00-2010 to 00-00-2010**

4. TITLE AND SUBTITLE
Multifunctional Poly(2,5-benzimidazole)/Carbon Nanotube Composite Films

5a. CONTRACT NUMBER
5b. GRANT NUMBER
5c. PROGRAM ELEMENT NUMBER

6. AUTHOR(S)

5d. PROJECT NUMBER
5e. TASK NUMBER
5f. WORK UNIT NUMBER

7. PERFORMING ORGANIZATION NAME(S) AND ADDRESS(ES)
Ulsan National Institute of Science and Technology (UNIST),Interdisciplinary School of Green Energy & Inst of Advanced Materials & Devices,100, Banyeon,Ulsan 689-798, South Korea,

8. PERFORMING ORGANIZATION REPORT NUMBER

9. SPONSORING/MONITORING AGENCY NAME(S) AND ADDRESS(ES)

10. SPONSOR/MONITOR'S ACRONYM(S)
11. SPONSOR/MONITOR'S REPORT NUMBER(S)

12. DISTRIBUTION/AVAILABILITY STATEMENT
Approved for public release; distribution unlimited

13. SUPPLEMENTARY NOTES

14. ABSTRACT

The AB-monomer, 3,4-diaminobenzoic acid dihydrochloride was recrystallized from an aqueous hydrochloric acid solution and used to synthesize high-molecular-weight poly(2,5- benzimidazole) (ABPBI). ABPBI/carbon nanotube (CNT) composites were prepared via in situ polymerization of the AB-monomer in the presence of single-walled carbon nanotube (SWCNT) or multiwalled carbon nanotube (MWCNT) in a mildly acidic polyphosphoric acid. The ABPBI/SWCNT and ABPBI/MWCNT composites displayed good solubility in methanesulfonic acid and thus uniform films could be cast. The morphology of these composite films was studied by X-ray diffraction, scanning electron microscopy transmission electron microscopy, and atomic force microscopy. The results showed that both types of CNTs were uniformly dispersed into the ABPBI matrix. Tensile properties of the composite films were significantly improved when compared with ABPBI, and their toughness (200 MPa) was close to the nature?s toughest spider silk (215 MPa). The electrical conductivities of ABPBI/SWCNT and ABPBI/MWCNT composite films were 9.10 10 5 and 2.53 10 1 S/cm, respectively, whereas that of ABPBI film was 4.81 10 6 S/cm. These values are 19 and 52,700 times enhanced by the presence of SWCNT and MWCNT, respectively. Finally, without acid impregnation, the ABPBI film was nonconducting while the SWCNT- and MWCNT-based composites were proton conducting with maximum conductivities of 0.018 and 0.017 S/cm, respectively.

15. SUBJECT TERMS

16. SECURITY CLASSIFICATION OF:			17. LIMITATION OF ABSTRACT	18. NUMBER OF PAGES	19a. NAME OF RESPONSIBLE PERSON
a. REPORT	b. ABSTRACT	c. THIS PAGE			
unclassified	**unclassified**	**unclassified**	**Same as Report (SAR)**	**12**	

achieve homogeneous dispersion of CNTs in various matrix materials via physical methods aided by sonication,[10] chemical methods using strong and oxidizing acids, such as sulfuric acid and nitric acid,[11] or procedures combined with applying sonication.[12] However, applying sonication often results in structural damages such as sidewall opening, breaking, and tubes being turning into amorphous carbon.[13] Treatment in strong acids, specifically in nitric acid as a strong oxidizing agent, turns CNTs into CNT oxides, which lose not only electrical conductivity but also structural integrity.[14] Furthermore, even after achieving homogeneous dispersion, a strong interfacial adhesion between CNT and polymer matrix is required.[15] A simple melt or solution mixing of polymer with CNT may not be an efficient way for the homogeneous dispersion and effective wetting without chemically and/or physically chopping CNTs into shorter tubes. This results in reduced aspect ratio.[16] Hence, controlled covalent grafting of polymer onto the surface of CNT without or with minimal damage[17] and/or *in situ* polymerization of corresponding monomer in the presence of CNT are probably better routes for attaining strong interfacial interaction and thus strengthening the reinforcement effect.[18]

We have developed one-pot purification and functionalization of carbon nanomaterials in a mild reaction medium comprising polyphosphoric acid (PPA) with additional phosphorous pentoxide (P_2O_5).[19] This has been proven to be a nondestructive reaction medium that does not damage CNT framework. It is also strong enough to promote efficient Friedel-Crafts-type polycondensation. Commercial grade PPA, which contains 83 wt % phosphorous pentoxide, has been optimized and used as a superior polymerization medium for the synthesis of high-performance polybenzazoles (PBXs) such as rigid-rod polymers: polybenzobisthiazole (PBZT), polybenzobisoxazole (PBO), and polybenzobisimidazole (PBI), and rigid coil polymers: poly(2,5- or 2,6-benzooxazoles) (ABPBO) and poly(2,5-benzimidazole) (ABPBI).[20] Although a few PBX/CNT composites derived from *in situ* polycondensation in PPA have been reported,[21] the one-pot purification of SWCNT and preparation of composites via *in situ* polymerization have not been reported. Furthermore, all previously reported approaches may incur structural damage of CNT framework by applying sonication and/or strong acid treatments. As a result, the electrical conductivity of PBX/CNT composites has not yet been optimized.[9f]

Herein, we report an *in situ* self-condensation of diprotonated AB-monomer, namely 3,4-diaminobenzoic acid dihydrochloride, for the synthesis of ABPBI in the presence of SWCNT or MWCNT in an optimized PPA. The composite films were then evaluated for their thermal and mechanical as well as electrical and proton-conducting properties.

RESULTS AND DISCUSSION

Among PBXs, PBIs are known for their outstanding thermal stability, mechanical and electrical properties, and chemical resistance.[22] They are currently used as thermal insulating materials and have potential applications as high-strength fibers,[23] gas separation, and fuel cell membranes.[24] Yet, in spite of extensive work in rigid-rod PBI, there are few reports on rigid-coil ABPBI.[25] Among the PBI family, ABPBI has the simplest structure and can be easily prepared from a single, inexpensive, and commercially available AB-monomer, that is, 3,4-diaminobenzoic acid (DABA), via polycondensation in PPA. Hence, it has recently attracted much attention as an emerging material for high-temperature fuel cell membrane to replace the expensive and electrochemically less stable Nafion family.[25]

In Situ Polymerization

The synthesis of poly(2,5-benzimidazole), which is also known as ABPBI, has been reported in early 1960s.[22(a),26] However, the molecular weights of ABPBI, when it is prepared from as-received AB monomer, namely 3,4-diaminobenzoic acid available from several commercial sources with purity 95–97%, are relatively low with inherent viscosity (1.4–2.7 dL/g) in concentrated sulfuric acid at 30 °C.[25,27] It is also known that polymerization of rigorously purified 3,4-diaminobenzoic acid in either phosphoric acid/P_2O_5[28] or methanesulfonic acid/P_2O_5[29] mixtures has led to high-molecular-weight ABPBI. In this study, commercial 3,4-diaminobenzoic acid was recrystallized from an aqueous hydrochloric acid solution (water/concentrated hydrochloric acid, 90/10, v/v) to yield highly pure 3,4-diaminobenzoic acid dihydrochloride (purity $>$ 99.99+%, HPLC). In fully protonated form, it is expected that 3,4-diaminobenzoic acid would have longer shelf-life than in acid-free form. In addition, we surmise that hydrochloric acid, which can be *in situ* generated at room temperature during the slow dehydrochlorination of dihydrochloride monomer, could raise the acidity of the reaction medium that might improve both the dispersion and purification of CNTs by optimized PPA. Specifically, as-prepared SWCNT contains various impurities such as metallic particles, carbonaceous impurities, and amorphous carbons. The acidity of gaseous hydrochloric acid ($pK_a \sim -8$) is many orders of magnitude stronger than PPA (pK_a of H_3PO_4 or orthophosphoric acid ~ 2) and thus, the population of protonated on the surface of CNT under such conditions should be higher, making the solvation of CNT in PPA more effective.[30] After dehydrochlorination is completed by stepwise heating from room temperature to 150 °C in PPA, the reaction mixture is further heated to 175 °C for 3 h to ensure complete imidazole ring closure, resulting in high-molecular-weight ABPBI [Fig. 1(a)].[31]

For the concurrent dispersion and purification of CNT in PPA and the polymerization of the AB monomer in one-pot process to generate *in situ* ABPBI/CNT composites, the polycondensation of the 3,4-diaminobenzoic acid dihydrochloride was carried out in the presence (10 wt % based on the monomer feed) of SWCNT or MWCNT [Fig. 1(b)]. The initial color of all reaction mixtures was black because of the SWCNT or MWCNT dispersion. The color then became dark, shinny brown as polymerization progressed, which was taken as an indication for the homogeneous dispersion of CNTs. In both cases, the reaction mixtures were homogeneous with drastic increase in viscosity, when reaction temperature was approaching 150 °C. However, the solution

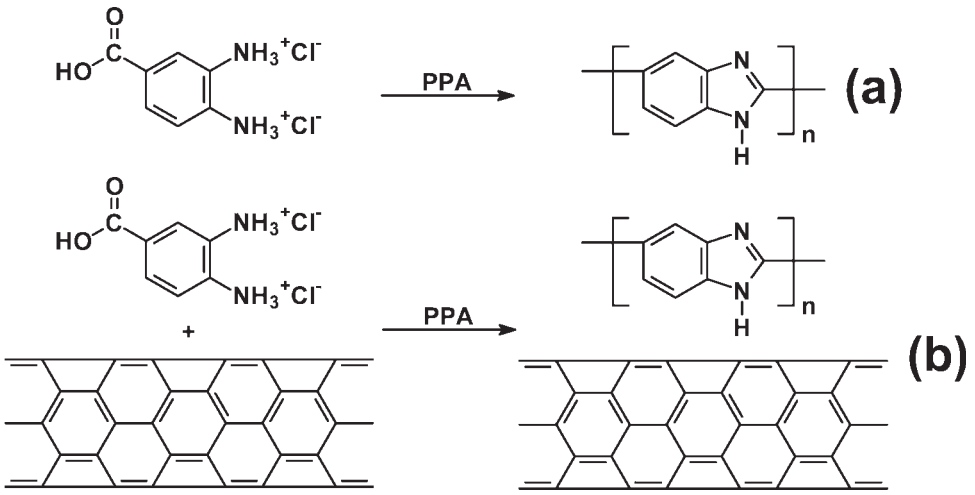

FIGURE 1 (a) Synthesis of poly(2,5-benzimidazole) (ABPBI) in polyphosphoric acid (PPA) at 175 °C; (b) *in situ* polymerization of 3,4-diaminobenzoic acid dihydrochloride as an AB monomer in the presence of single-walled carbon nanotube (SWCNT) or multi-walled carbon nanotube (MWCNT) to generate corresponding ABPBI/CNT composites.

behaviors of final reaction mixtures were clearly different between ABPBI and ABPBI/CNT composites. The ABPBI mixture at 175 °C was too viscoelastic to have efficient flow, and it was difficult to spin a fiber by simply pouring its hot polymerization dope into distilled water. On the other hand, both CNT-containing reaction mixtures at the similar temperature flowed quite well to yield long fibers upon similar workup. All isolated products were then Soxhlet extracted with water for 3 days to ensure the complete removal of residual PPA. They were further Soxhlet extracted with methanol for 3 days for the removal of other low molar mass impurities and then freeze dried. The intrinsic viscosity of resultant ABPBI was ~5.23 dL/g [MSA, 30 ± 0.1 °C; see Fig. S1(a) in Supporting Information], which is higher than literature values (1.4–2.7 dL/g in 96% sulfuric acid at 30 °C).[25] The intrinsic viscosities of ABPBI/SWCNT and ABPBI/MWCNT composites were 6.61 and 5.31 dL/g (MSA, 30 ± 0.1 °C), respectively [see Fig. S1(b,c) in Supporting Information], and these values are higher than that of ABPBI. It is important to point out that the dilute solutions, in terms of reduced and inherent viscosities, of both ABPBI/SWCNT and ABPBI/MWCNT composites have behaved very similar to that of ABPBI. This comparison not only implicates that the polycondensation of the AB-monomer was not affected by the presence of CNTs but also a strong polymer-CNT interaction (i.e., polymer wrapping) exists for these composites.

In all cases, final yields were higher than maximum calculated yields even after complete workup procedures. This discrepancy might be related to the hygroscopic nature of ABPBI. Likewise, the large discrepancy between theoretical and experimental CHN contents in elemental analysis (Table 1) should also be attributed to bounded water in ABPBI (see Fig. S2 and Table S1 in Supporting Information). ABPBI/SWCNT composite showed relatively larger discrepancy of C content, and it was presumably due to the low carbon content of as-received SWCNT (see Table 1).

FTIR Study

The transmittance of CNT samples was very poor due to the fact that CNTs strongly absorb infrared light [Fig. 2(a,b)]. They did not show comparable peaks at the same degree of magnification, whereas ABPBI, SWCNT/ABPBI, and MWCNT/ABPBI displayed a strong and broad ν(OH) around 3500 cm^{-1}, which is attributed largely to the bounded water in hygroscopic ABPBI (see Fig. S2 in Supporting Information). There are characteristic C═N and C—N stretching bands at 1628 and 1287 cm^{-1}, respectively, (Fig. 2), which are assignable to the imidazole moiety of ABPBI polymer. The peaks from 3500 to 3300 cm^{-1} were attributed to the isolated N—H stretch of the imidazole ring, whereas the broad band near 3300–3150 cm^{-1} is due to intermolecular hydrogen-bonded H···N···H structures, and it becomes broader in the presence of moisture. The only difference between ABPBI and ABPBI/CNT composites was the relative intensity of respective peaks. There were no discernable characteristic peaks among samples (Fig. 2).

Raman spectra showed that the ratios of D/G band intensity (I_D/I_G) of ABPBI/SWCNT and ABPBI/MWCNT were increased because of the ABPBI coating on the surface of CNT (see Fig. S3 in Supporting Information).

Thermal Properties

The thermograms obtained from differential scanning calorimetry (DSC) characterization are not included in this article, because ABPBI has expectedly its transition temperature higher than its degradation temperature.[22(a)] In all cases, the thermograms showed featureless traces, except for a broad endothermic peak around 150 °C, which is caused by the release of polymer-bounded water from the sample.

To minimize effect from the contribution of bounded water, all samples were annealed in the chamber of thermogravimetric analyzer (TGA) at 300 °C for 10 min before analysis. After cooled down to room temperature, the samples were

TABLE 1 Thermogravimetric (TGA) and Elemental Analysis (EA) Data

	TGA[a]				Elemental Analysis			
	In Air		In N_2			C (%)	H (%)	N (%)
Sample	$T_{d5\%}$ (°C)	Char 800 °C (%)	$T_{d5\%}$ (°C)	Char 800 °C (%)				
ABPBI	611	42.3	656	86	Calcd.	72.40	3.47	24.12
					Found	57.01	4.58	19.07
SWCNT	371	57	623	71.0	Calcd.	100.00	0.00	0.00
					Found	82.84	0.74	–[b]
MWCNT	574	~0	789	94.6	Calcd.	100.00	0.00	0.00
					Found	97.81	0.30	–[b]
ABPBI/SWCNT	578	11.2	658	88	Calcd.	77.29	2.86	19.85
					Found	61.56	3.86	16.88
ABPBI/MWCNT	607	26.6	668	88	Calcd.	77.29	2.86	19.85
					Found	64.80	3.84	15.87

[a] The temperature at which 5% weight loss ($T_{d5\%}$) occurred on TGA thermogram obtained with a heating rate of 10 °C/min.
[b] Below detection limit.

heated to 800 °C with the ramping rate of 10 °C/min for experiments conducted in both air and nitrogen. The ABPBI, SWCNT, MWCNT, SWCNT/ABPBI, and MWCNT/ABPBI samples showed that the temperature at which 5% weight loss ($T_{d5\%}$) in air occurred at 574, 371, 611, 607, and 578 °C, in that order [Fig. 3(a) and Table 1). Among these samples, SWCNT started to decompose at the lowest temperature, presumably because of the thermooxidative instability (combustion) of amorphous carbon. It should be noted that the char yield of as-received SWCNT at 800 °C was 57%, whereas that of MWCNT was practically 0%. The high-residue yield of SWCNT at 800 °C in air is most probably due to more combustion-resistant impurities, such as metallic catalyst particles and crystalline carbonaceous impurities [see Fig. S4(a) in Supporting Information].[32] Surprisingly, ABPBI homopolymer displayed the highest thermooxidative stability among the samples in air ($T_{d5\%}$ = 611 °C), which is 240 and 37 °C higher than those of as-received SWCNT ($T_{d5\%}$ = 371 °C) and MWCNT ($T_{d5\%}$ = 574 °C), respectively. In contrast to the expectation, ABPBI turned out to be the component that had improved thermooxidative stability of the ABPBI/CNT composites. The comparison of char yields at 800 °C in air could be considered as a qualitative assessment of SWCNT purity. Taking into account the loaded SWCNT amount (10 wt %), ABPBI/SWCNT was expected to display higher char yield (11.2%) at 800 °C than those of ABPBI (42.3%) and ABPBI/MWCNT (26.6%). However, the amount of residues was the lowest among them, implying that the tenacious (and thermooxidatively stable) impurities present in as-received SWCNT were almost all removed during the polymerization and workup stages [see Fig. S3(b–d) in Supporting Information]. This rationalization implicated that a mildly acidic PPA medium with additional hydrochloric acid, which was *in situ* generated from AB monomer, might be an efficient way for the purification of as-received SWCNT.[19(b)]

Under nitrogen atmosphere, as-received MWCNT apparently was the most stable with $T_{d5\%}$ at 789 °C and char yield at 800 °C was 94.6 wt % [Fig. 3(b)]. Unlike under air atmosphere, as-received SWCNT displayed better thermal stability in nitrogen. It had $T_{d5\%}$ at 623 °C, and its char yield at 800 °C was 71.0 wt %. The $T_{d5\%}$'s of ABPBI, ABPBI/SWCNT, and ABPBI/MWCNT at 800 °C were similar at 656, 658, and 668 °C, corresponding to char yield of 86, 88, and 88 wt %, respectively.

Scanning Electron Microscopy

A small portion of warm ABPBI dope at the end of polymerization was placed in a Petri dish, which was then placed on a leveled hot plate to form uniform film. After cooled to room temperature, the dish was immersed in distilled water to let PPA diffuse out from the dope into the water to result in a coagulated, porous ABPBI film. This film was further Soxhlet extracted with water and methanol. The SEM images of the resulting ABPBI film show that the surface texture consists of uniformly distributed fibrils [Fig. 4(a)], indicating that high-molecular-weight ABPBI has been indeed obtained. Similarly, the porous films of ABPBI/SWCNT and ABPBI/MWCNT were also prepared, and their SEM images obtained from fracture surfaces are quite different from that of ABPBI. The ABPBI/SWCNT shows relatively round-shaped morphology [Fig. 4(c)], whereas ABPBI/MWCNT shows relatively sharp fibril structure [Fig. 4(e)]. In both cases, the degree of CNT dispersion cannot be judged, because CNTs are well blended in ABPBI matrix and the presence of CNTs cannot be clearly discerned with SEM images.

All SEM images obtained from the fracture surfaces of sample films cast from MSA solutions (see Experimental section) display similar morphology [Fig. 4(b,d,f)]. ABPBI shows dense fibril surface [Fig. 4(b)]. Because of the diameter dimension of individual SWCNT (<2 nm), the presence of

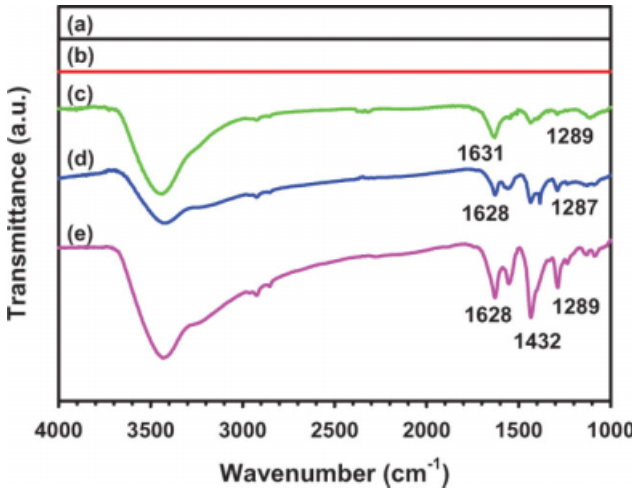

FIGURE 2 FTIR (KBr pellet) spectra: (a) SWCNT; (b) MWCNT; (c) ABPBI/SWCNT composite; (d) ABPBI/MWCNT composite; and (e) ABPBI. [Color figure can be viewed in the online issue, which is available at www.interscience.wiley.com.]

SWCNT from the fracture surface is inconclusive by SEM at this magnification [Fig. 4(d)]. On the other hand, the fractured surface of ABPBI/MWCNT composite film shows that MWCNT is well dispersed in the ABPBI matrix [Fig. 4(f)]. Upon greater magnification, it is quite clear that the interface between ABPBI and MWCNT is not discernable [Fig. 4(f), inset], indicating that ABPBI and MWCNT are well bounded to each other (see also TEM images in Fig. S4 and AFM images in Fig. S5 in Supporting Information).

WAXS Patterns

To assess the dispersion quality of CNTs in ABPBI matrix, wide-angle X-ray scattering (WAXS) patterns were obtained from powder samples without applied strain. In the case of ABPBI homopolymer, two characteristic peaks at $2\theta = 11.0°$ and 25.91° with respective to *d*-spacings = 8.03 and 3.46 Å were detected (Fig. 5 and Table 2). The characteristic peak centered at about 25.91°, which corresponds to a *d* spacing of 3.46 Å, is assignable to the stacking of ABPBI chains.[33] Detected side-by-side, the interplane distance was slightly increased from the literature value at 3.39–3.41 Å because the polymer chains in powder sample were less tightly packed [Fig. 5(a)]. Interestingly, the ABPBI homopolymer prepared for this study displayed an additional strong peak that appeared at $2\theta = 11.00°$ (8.03 Å). It was an indication of more ordered structure, because the sample workup procedure was done thoroughly, and the residual reaction medium should have been completely removed (see Experimental section). On the basis of peak width and sharpness reported in the literature,[34] it appeared that a significant amount of residual phosphoric acid still remained in ABPBI, and it could play as an extraneous agent to disturb molecular orientation.

ABPBI/SWCNT composite displayed similar WAXS pattern to that of ABPBI [Fig. 5(b)]. The 2θ (*d*-spacing) values for both interplane π–π distance and oriented structure were slightly shifted to 10.76° (8.22 Å) and 26.01° (3.42 Å), respectively. In the case of ABPBI/MWCNT composite, a typical 2θ (*d*-spacing) from interplane π–π distance attributed to both ABPBI and MWCNT was 25.72° (3.46 Å), which was shifted by 0.19° (0.01 Å) when compared with that from ABPBI homopolymer [Fig. 5(c)]. The two peaks appeared from ABPBI homopolymer at 9.05° (9.77 Å) and 20.85° (4.26 Å) had merged into a single peak at 13.9° (6.36 Å).

UV-Absorption and Emission Spectra

The photograph shown in Figure 6(a) is a visual demonstration as an additional support for our claim of the homogeneous dispersion of CNTs in ABPBI matrix. The ABPBI, ABPBI/SWCNT, and ABPBI/MWCNT samples were completely soluble in MSA (no CNT agglomerates visually detectable in the composite samples). They emitted strong blue light when exposed to a UV light (365 nm) from a hand-held lamp at ~1 foot away [Fig. 6(a, i–iii)]. The composite solutions were

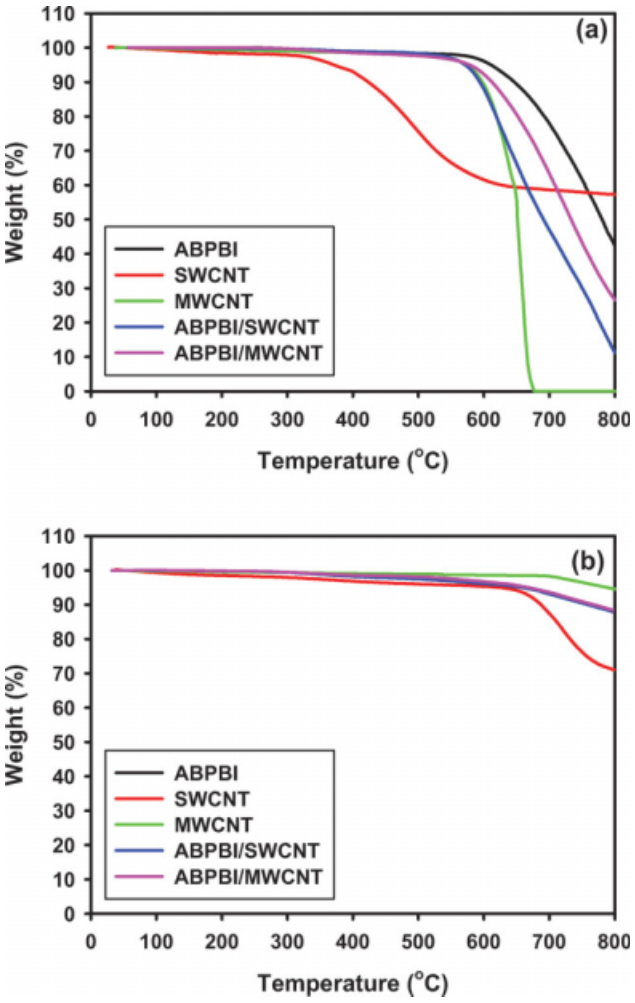

FIGURE 3 TGA thermograms obtained with a heating rate of 10 °C/min after annealing samples at 300 °C for 10 min: (a) in air and (b) in nitrogen. [Color figure can be viewed in the online issue, which is available at www.interscience.wiley.com.]

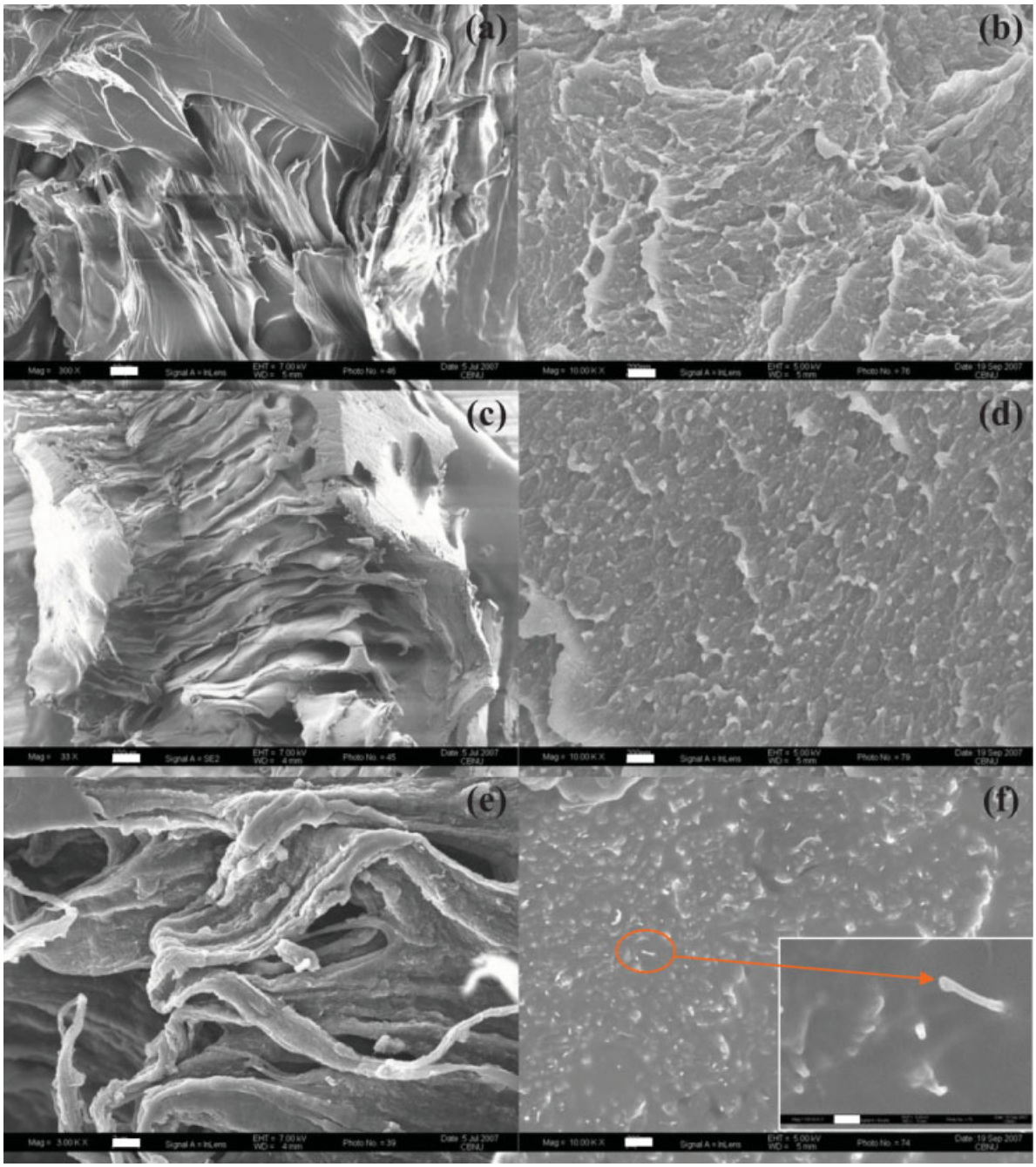

FIGURE 4 SEM images of samples: (a) the fracture surface of ABPBI film directly cast from reaction mixture (×300, scale bar is 20 μm); (b) the fractured surface of ABPBI film cast from MSA solution (×10,000, scale bar is 600 nm); (c) the fracture surface of ABPBI/SWCNT composite film directly cast from reaction mixture (×33, scale bar is 200 μm); (d) the fractured surface of ABPBI/SWCNT composite film cast from MSA solution (×10,000, scale bar is 600 nm); (e) the fracture surface of MWCNT/ABPBI composite film directly cast from reaction mixture (×3000, scale bar is 2 μm); and (f) the fractured surface of MWCNT/ABPBI composite film cast from MSA solution (×10,000, scale bar is 600 nm). The scale bar for the inset is 100 nm. [Color figure can be viewed in the online issue, which is available at www.interscience.wiley.com.]

homogeneous and optically clear, whereas MWCNT and SWCNT solutions contained CNT agglomerates that were easily seen by a naked eye [Fig. 6(a, iv,v)]. To further substantiate the homogeneous dispersion of CNTs in the composite samples, UV-absorption curves were obtained from their basic solutions in *N*-methyl-2-pyrrolidinone (NMP). As ABPBI is only soluble in strong acids such as sulfuric acid, MSA, and trifluoromethanesulfonic acid, UV-absorption was measured by adding a drop of MSA into its NMP solution. The absorption spectrum of protonated ABPBI consists of a strong band

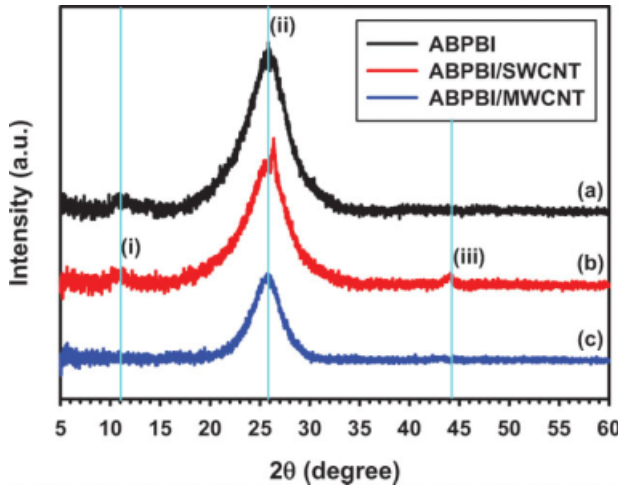

FIGURE 5 XRD patterns of samples: (a) ABPBI; (b) ABPBI/SWCNT; and (c) ABPBI/MWCNT.

at 415 nm with a shoulder at 382 nm [Fig. 6(b)]. ABPBI/SWCNT and ABPBI/MWCNT composites display very similar spectra, indicating that the ground-state band structure of ABPBI in composites is almost identical as that of a free ABPBI.

The emission spectra of the ABPBI and its CNT composite solutions are given in Figure 6(c). The maximum emission wavelength (λ_{max}) of ABPBI was 518 nm. In the case of composites, the emission spectra with different intensities, which were dependent on the concentration of ABPBI, were almost identical to that of neat ABPBI, implying that the excited-state properties of ABPBI in the presence of CNT are also more or less unaffected. Overall, these results may also be taken as a support for our belief that the dispersion of CNTs is uniform in ABPBI matrix.

Mechanical Properties

Cast films (see Fig. S6 in Supporting Information) were cast from MSA solution and cut into specimens with size 5 mm × 70 mm and thickness 0.35–0.45 mm. Representative stress–strain curves of samples are presented in Figure 7, and the data are summarized in Table 3. The tensile strength, modulus, elongation, and toughness of ABPBI film were 25 MPa, 0.88 GPa, 490%, and 101.0 MPa, respectively. These values are very much different from the semirigid PBI prepared from AA+BB polymerization.[35] Specifically, elongation value was increased by almost one order of magnitude compared with the literature value.[35] The result could be due to the much higher molecular weight ([η] = 5.23 dL/g) and polymer-bounded water in ABPBI. Although the former would mainly contribute to high strain-to-break value, but the influence of trapped moisture (plasticizing effect) could not be excluded. Tensile test results are generally quite subjective to the sample conditions, and therefore, the amount

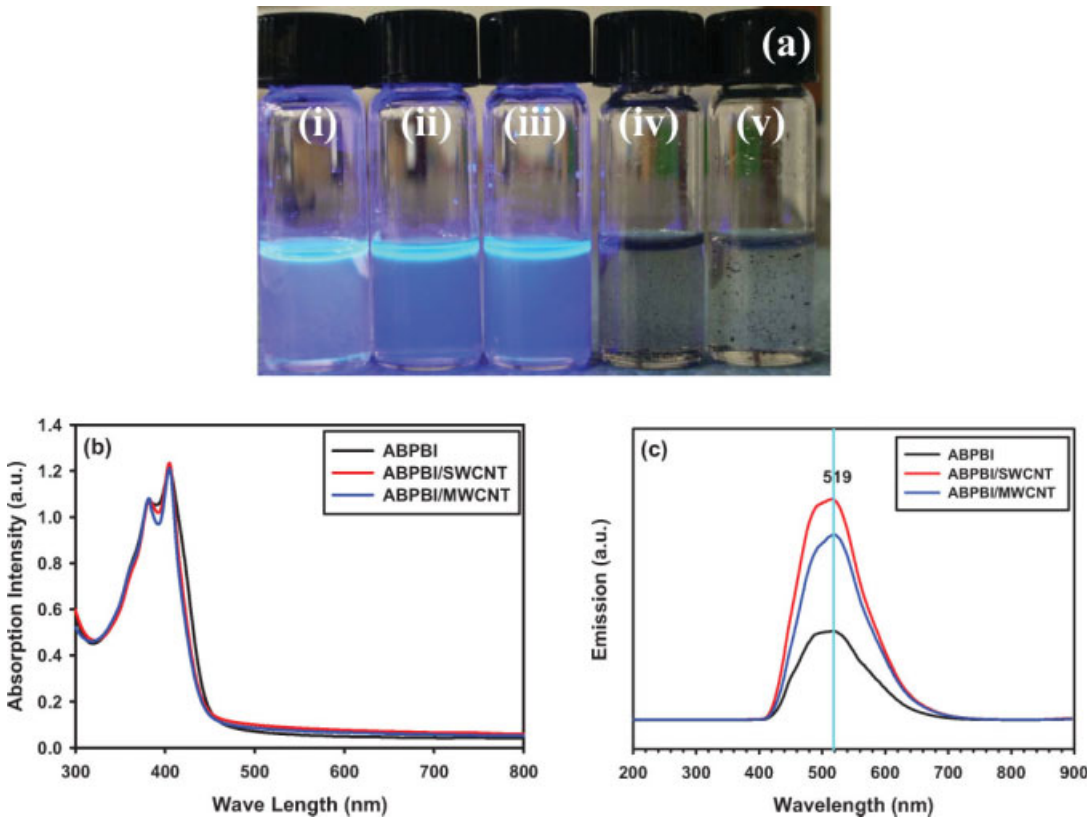

FIGURE 6 (a) Digital photograph of sample solutions in MSA under 365 nm UV light; (b) UV-absorption spectra of samples in NMP with a drop of MSA; and (c) emission spectra of samples in NMP with a drop of MSA. Excitation wavelength was 415 nm: (i) ABPBI; (ii) ABPBI/SWCNT; (iii) ABPBI/MWCNT; (vi) SWCNT; and (v) MWCNT.

TABLE 2 XRD Analysis Data of Film Samples

	i		ii		iii	
Sample	2θ (°)	*d*-Spacing (Å)	2θ (°)	*d*-Spacing (Å)	2θ (°)	*d*-Spacing (Å)
ABPBI	11.00	8.03	25.91	3.46	–	–
ABPBI/SWCNT	10.76	8.22	26.01	3.42	43.87	2.06
ABPBI/MWCNT	–	–	25.72	3.46	–	–

of bound water in the hygroscopic ABPBI sample could be another significant factor for the tensile properties measured, as the bound water can act as a plasticizer making ABPBI softer. The amount of trapped moisture can be determined by TGA (see Fig. S2 and Table S1 in Supporting Information). Although the residual water could be removed at elevated temperatures with/without applying vacuum, it is known that atmospheric moisture could be easily absorbed by hygroscopic ABPBI during sample preparation. Hence, all films were cast and dried at the same conditions so that the test results could be reasonable for meaningful comparison. Relative to ABPBI film, the tensile strengths of ABPBI/SWCNT and ABPBI/MWCNT composite films were significantly increased by as much as 60 and 84%, respectively. The tensile moduli of the composite films were also improved by as much as 61 and 74%, respectively. The elongation values of ABPBI/SWCNT and ABPBI/MWCNT were improved by 61 and 25%, respectively. Toughness was calculated from the area under the stress–strain curve. The ABPBI/SWCNT and ABPBI/MWCNT films had the average toughness of 210 and 200 MPa, respectively, which were increased by 108 and 98% when compared with that of ABPBI film (101 MPa). Although film and fiber properties could not be directly compared, the values are close to the nature's toughest spider silk (~215 MPa).[36] Thus, this notable improvement of tensile properties could be attributable to not only the higher molecular weight of ABPBI attained in this work but also the strong interactions between ABPBI and CNT (see SEM images in Fig. 4 and TEM images in Fig. S4 in Supporting Information).

Electrical Conductivity of Films

The dc electrical conductivity of ABPBI homopolymer film was 4.81×10^{-6} S/cm, which was close to being an insulating material (Table 3). The ABPBI/SWCNT and ABPBI/MWCNT composite films showed 9.10×10^{-5} and 2.53×10^{-1} S/cm, respectively. ABPBI/SWCNT composite film was expected to display the better electrical conductivity, as SWCNT has the higher aspect ratio. Surprisingly, it was several orders of magnitude lower than that of ABPBI/MWCNT, which was in the semiconducting region. The higher electrical conductivity of ABPBI/MWCNT could be because of following reasons: (1) SWCNT bundles might not be well exfoliated into individual tubes (see Fig. S4 in Supporting Information); (2) the purity of as-received SWCNT was only 30–40 wt %, and thus, the actual amount of SWCNT in the ABPBI/SWCNT composite would be much lower (~3–4 wt %) after *in situ* purification in PPA [see Fig. 3(a)]; (3) another possibility is that the template polymerization of AB monomer onto the surface of SWCNT provided higher wrapping coverage, and thus insulating it because of the comparable SWCNT radius (~1 nm) and coil radius of ABPBI (~2.1–2.7 nm). (see Fig. S7 in Supporting Information).

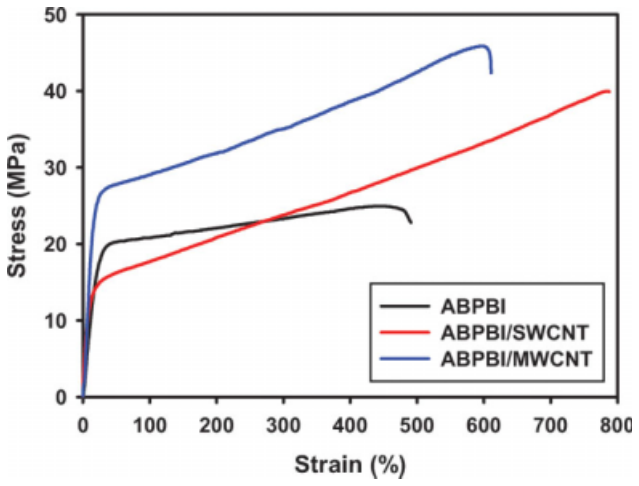

FIGURE 7 Representative stress–strain curves of samples, which were tested at 20 °C and relative humidity of 50%. The crosshead speed was 100% of gauge length per minute. [Color figure can be viewed in the online issue, which is available at www.interscience.wiley.com.]

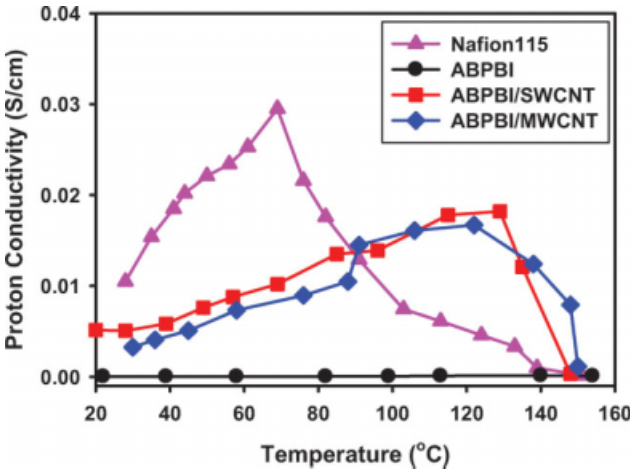

FIGURE 8 Proton conductivity of sample films, which was measured at relative humidity of 50%. [Color figure can be viewed in the online issue, which is available at www.interscience.wiley.com.]

TABLE 3 Tensile Properties and Electrical Conductivity of Film Samples

	Tensile Properties[a]				
Sample	Strength (MPa)	Modulus (GPa)	Strain (%)	Toughness (MPa)	Electrical[b] Conductivity (S/cm)
ABPBI	25 ± 2	0.88 ± 0.1	490 ± 44	101.0 ± 13.8	$4.81 \times 10^{-6} \pm 8.6 \times 10^{-7}$
ABPBI/SWCNT	40 ± 3	1.42 ± 0.2	788 ± 80	210.0 ± 23.0	$9.10 \times 10^{-5} \pm 8.0 \times 10^{-6}$
ABPBI/MWCNT	46 ± 4	1.53 ± 0.2	611 ± 58	200.0 ± 19.6	$2.53 \times 10^{-1} \pm 1.0 \times 10^{-2}$

[a] Tensile properties were averaged values of five tests out of seven samples after the best and worst tests were discarded. Toughness was calculated from the area under the stress–strain curve in tensile test. Samples are tested at 20 °C with 50% relative humidity. The crosshead speed was 100% of gauge length per minute.

[b] Electrical conductivity is an average value of 20 measurements at 20 °C with 50% relative humidity.

Proton Conductivity of Films

The proton conductivity was determined with two-point probe conductivity measurement at the relative humidity of 50% (Fig. 8). For benchmarking, Nafion 115 was also evaluated under the same measuring conditions and found to display higher proton conductivity (maximum 2.95×10^{-2} S/cm at 70 °C). However, the conductivity of Nafion 115 began to drop drastically when the temperature was raised near and above 70 °C. On the other hand, ABPBI showed an initial value of 3.75×10^{-5} S/cm at 22 °C, which gradually increased as the temperature was increased, up to 1.42×10^{-4} S/cm at 140 °C before the conductivity decay started. Expectedly, the low proton conductivity of ABPBI when compared with Nafion 115 could be explained in terms of their acidity difference. The pK_a values of Nafion 115 and ABPBI are about 6[37] and 12.75 (for benzimidazole, but for ABPBI, pK_a value is expected to be lower because of conjugative effect in the polymer backbone),[38] respectively. Thus, their pK_a difference is ~18 orders of magnitude, but the difference in their maximum proton conductivities is only two orders of magnitude. It appears that in ABPBI, there is a nonlinear relationship between the acidity (at the molecular level) and proton conductivity (in the bulk state), and rather surprisingly at first, there is less temperature dependence in its proton conductivity as well. We suspect that the unique features of ABPBI, namely (i) large number of benzimidazoles per polymer chain, (ii) most of benzimidazole protons should be aligned along the ABPBI chain (see Fig. 1), and (iii) the extended conjugation in ABPBI chain that could induce high proton mobility via tautomerization across repeat units, may be the contributing factors. Further, as the dissociation of proton from benzimidazole is a function of temperature as opposed to the complete ionization of sulfonic group at room conditions (provided that enough water are present), it is reasonable to assume that the concentration of mobile protons in ABPBI would increase with an increase in the surrounding temperature. Still, the proton conductivity of ABPBI is too low to be used as fuel cell membrane. To improve its proton conductivity, phosphoric acid or other mineral acids are impregnated into ABPBI matrix, which results in not only the poor mechanical properties of ABPBI membrane but also acid migration to the surface of the membrane.[36]

The maximum proton conductivity of ABPBI/SWCNT is 0.018 S/cm. The value is slightly higher than that (0.017 S/cm) of ABPBI/MWCNT. However, the proton conductivities of ABPBI/CNT films without acid doping are improved by approximately two orders of magnitude over that of ABPBI film (see Table 3). We suspect that the relatively high proton conductivity of ABPBI/CNT composite films could be originated from the proton channels along the interface of ABPBI and CNT and/or inner channel of CNT. Although further study is necessary to prove this speculation, the ABPBI/SWCNT composite film[39] could be a good candidate for proton-conducting membranes without the need for acid impregnation.

CONCLUSIONS

Multifunctional ABPBI/CNT composites were prepared via *in situ* polymerization of "protonated" AB monomer. CNTs did not affect the polymerization of AB monomer to yield high-molecular-weight ABPBI in a mildly acidic PPA medium at 175 °C for 3 h. CNTs remained structurally intact during *in situ* polycondensation process and under subsequent workup conditions. It could be concluded that the reaction condition was indeed feasible for the purification (more so for SWCNT than MWCNT) and dispersion of CNTs as well as polymerization of the AB monomer in a one-pot process. The homogeneous dispersion of CNTs in ABPBI matrix was visually confirmed by SEM imaging experiments. As a result, considerable improvement of mechanical properties of ABPBI/CNT films over ABPBI film could be achieved. On the basis of SEM data, we interpret that the surfaces of SWCNT and MWCNT have been decorated well with ABPBI, and because the boundary between ABPBI and CNT phases could not be discernable, homogeneous CNT dispersion in the ABPBI matrix has been achieved. Thus, load transfer from ABPBI to CNT should be efficient to result in the enhanced mechanical properties of composite films, especially the toughness. Among these films, ABPBI/MWCNT displayed the best electrical conductivity. ABPBI/CNT composites also showed proton conductivities without acid impregnation. Thus, electrically conducting, proton conducting, thermally stable, and tough multifunctional materials were prepared.

Subject to further improvement, they are potentially useful for various applications for areas, where require affordable, lightweight, and high-performance materials.

EXPERIMENTAL

Materials

All reagents and solvents were purchased from Aldrich Chemical or Tokyo Chemical and used as received, unless otherwise specified. The AB monomer, 3,4-diaminobenzoic acid, was recrystallized from 10 vol % (conc. HCl/H_2O, v/v) aqueous hydrochloric acid to give 3,4-diaminobenzoic acid dihydrochloride (HPLC purity $>$ 99.99+%, m.p. $>$ 300 °C dec.). Both single-walled carbon nanotube (SWCNT, 30–40 wt % purity) and multiwalled carbon nanotube (MWCNT, CVD MWCNT 95 with diameter of ~20 nm and length of 10–50 μm) were obtained from Hanhwa Nanotech, Seoul, Korea.[40]

Instrumentation

The melting points (m.p.) were determined on a Mel-Temp melting point apparatus and are uncorrected. Intrinsic viscosities were determined using Cannon-Ubbelohde No. 200 viscometer. Flow times were recorded for MSA solution, and polymer concentrations were ~0.5–0.1 g/dL at 30.0 ± 0.1 °C. Fourier transform infrared (FTIR) spectra were recorded on a Jasco FTIR 480 Plus spectrophotometer. Solid samples were imbedded in KBr disks. Elemental analyses were performed with a CE Instruments EA1110. Thermogravimetric analysis (TGA) was conducted in air and nitrogen atmospheres with a heating rate of 10 °C/min using a Perkin–Elmer TGA7 thermogravimetric analyzer with TAC7 controller. UV–vis spectra were obtained from a Perkin–Elmer Lambda 35 UV–vis spectrometer. Fluorescence studies were conducted with a Perkin–Elmer LS 55 fluorescence spectrometer. Applied excitation wavelength was UV absorption maximum of each sample. WAXS patterns were recorded on Scintag DMS2000 diffractometer. The field emission scanning electron microscopy (FESEM) was done by using LEO 1530FE. The field emission transmission electron microscope (FETEM) was used a FEI Tecnai G2 F30 *S*-Twin. Proton conductivity was evaluated using a two-point probe method with a Solartron 1260 AC impedance analyzer with amplitude of 10 mV and a frequency range of 1–100,000 Hz at relative humidity of 50%. Each film sample was fixed in a Teflon conductivity test cell consisted of a working and a reference Pt electrodes. The sample conductivity was determined by using $\sigma = (1/R)^*(L/A)$, where R is the resistance, L is the sample thickness, and A is the cross-sectional area. Surface resistivity of films was measured with AIT CMT-SR1000*N* four-point probe. Average values were taken after 20 measurements from different locations. Tensile tests were carried out on a universal testing machine (Instron model-UTM, DY-TSM-10). The crosshead speed was 100% of gauge length per minute at 20 °C and 50% humidity. Average values of five of seven tests were taken after the highest and lowest results were discarded. The images of atomic force microscope (AFM) were obtained from Veeco Multimode V. AFM samples were prepared by spin casting of polymer solution (a drop of MSA solution in 10 mL NMP) on silicon wafer. Energy minimized structures were performed by CS Chem 3D Std computational package (Version 8.0, Cambridge Soft Corp., Cambridge, MA).

Synthesis of Poly(2,5-benzimidazole)

Into a 250-mL resin flask equipped with a high torque mechanical stirrer, nitrogen inlet and outlet, 3,4-diaminobenzoic acid dihydrochloride (5 g, 22.2 mmol) and PPA (83% P_2O_5 assay; 50 g) were placed and stirred under a dry nitrogen purge at room temperature for 24 h to prevent drastic foaming caused by the release of hydrochloric acid gas. The color of heterogeneous mixture was red in the beginning. After 6 h, the color of opaque lump was changed to brown. When gas foaming was suppressed, the mixture was heated to 60 °C for additional 3 h to ensure complete dehydrochlorination. During this period, the mixture became transparent and light green colored. Then, the temperature was increased stepwise to 100 and 150 °C for 6 and 24 h, respectively. To ensure ring closure, the mixture was further heated to 175 °C for 3 h. Visually, an increase in the viscosity of reaction mixture was noted as the polymerization proceeded. At the end of polymerization, the mixture was cooled to room temperature and distilled water was added. Big chunks of polymeric product were isolated and subjected to Soxhlet extraction. The product was extracted with water for 3 days to completely remove acidic reaction medium and with methanol for 3 days to remove other low molar mass impurities, and finally freeze dried under reduced pressure (0.5 mmHg) for 48 h: $[\eta] = 5.23$ dL/g (MSA, 30 ± 0.1 °C). Anal. Calcd. for $C_7H_4N_2$: C, 72.40%; H, 3.47%; N, 24.12%, O, 0%. Found: C, 58.43%; H, 4.38%; N, 18.66%; O, 15.29%. The electrical conductivity of solution cast film: $4.81 \times 10^{-6} \pm 8.6 \times 10^{-7}$ S/cm.

In Situ Polymerization of 3,4-Diaminobenzoic Acid Hydrochloride with 10 wt % CNT Load

In the same setup for ABPBI synthesis, 3,4-diaminobenzoic acid dihydrochloride (4.5 g), as-received SWCNT (0.5 g) or MWCNT (0.5 g), and PPA (50 g) were placed. The rest of reaction sequence and workup procedure were the same as the synthesis of ABPBI homopolymer. The initial color of all reaction mixtures was black because of the SWCNT or MWCNT dispersion. At the end of the polymerization, the color of the mixture was dark shinny brown, and the mixture was poured into distilled water to form a long single filament. The resulting fibrous bundles were worked up following the same procedure for ABPBI homopolymer.

ABPBI/SWCNT composite: $[\eta] = 6.61$ dL/g (MSA, 30 ± 0.1 °C). Anal. Calcd. for $C_{8.08}H_4N_2$: C, 77.29%; H, 2.86%; N, 19.85%; O, 0%. Found: C, 59.23%; H, 3.48%; N, 15.72%; O, 12.27%. The electrical conductivity of solution cast film: $9.10 \times 10^{-5} \pm 8 \times 10^{-6}$ S/cm.

ABPBI/MWCNT composite: $[\eta] = 5.31$ dL/g (MSA, 30 ± 0.1 °C). Anal. Calcd. for $C_{8.08}H_4N_2$: C, 77.29%; H, 2.86%; N, 19.85%; O, 0%. Found: C, 64.73%; H, 3.75%; N, 16.29%; O, 12.58%. The electrical conductivity of solution cast film: $2.53 \times 10^{-1} \pm 0.01$ S/cm.

Film Casting

Films were cast from each composite sample (1.0 g) dissolved in methanesulfonic acid (MSA, 20 mL). The resultant homogeneous solutions were cast onto leveled glass plate in a custom-made film casting apparatus. MSA was slowly removed by heating the apparatus to 80 °C under reduced pressure (0.5 mmHg). The resultant uniform films were removed from glass plate after immersion in distilled water. They were sandwiched between Teflon membranes to make them flat and then kept under distilled water for 4 days. The films were further Soxhlet extracted with water for 3 days and methanol for additional 3 days to ensure complete removal of residual MSA. FTIR spectra of the films showed that there was no trace of residual MSA. The films were cut into size for property evaluation.

This work was supported by funding from US Air Force Office of Scientific Research, Asian Office of Aerospace R and D (AFOSR-AOARD), World Class University (WCU) supported by National Research Foundation (NRF), and Ministry of Education, Science and Technology (MEST) of Korea.

REFERENCES AND NOTES

1 Keller, T. Prog Struct Eng Mater 2001, 3, 132–140.

2 Ray, S. S.; Okamoto, M. Prog Polym Sci 2003, 28, 1539–1641.

3 Balazs, A. C.; Emrick, T.; Russell, T. P. Science 2006, 314, 1107–1110.

4 Ramanathan, T.; Abdala, A. A.; Stankovich, S.; Dikin, A. A.; Herrera-Alonso, M.; Piner, R. D.; Adamson, D. H.; Schniepp, H. C.; Chen, X.; Ruoff, R. S.; Nguyen, S. T.; Aksay, I. A.; Prud'homme, R. K.; Brinson, L. C. Nat Nanotech 2008, 3, 327–331.

5 Thostenson, E. T.; Ren, J. E.; Chou, T. W. Compos Sci Technol 2001, 61, 1899–1912.

6 Dimitrios, T.; Nikos, T.; Alberto, B.; Prato, M. Chem Rev 2006, 106, 1105–1136.

7 (a) Moniruzzaman, M.; Winey, K. I. Macromolecules 2006, 39, 5194–5205; (b) Fiedler, B.; Gojny, F. H.; Wichmann, M. H. G.; Nolte, M. C. M.; Schulte, K. Compos Sci Technol 2006, 66, 3115–3125; (c) Gao, J.; Zhao, B.; Itkis, M. E.; Bekyarova, E.; Hu, H.; Kranak, V.; Yu, A.; Haddon, R. C. J Am Chem Soc 2006, 128, 7492–7496; (d) Li, N.; Huang, Y.; Du, F.; He, X.; Lin, X.; Gao, H.; Ma, Y.; Li, F.; Chen, Y.; Eklund, P. C. Nano Lett 2006, 6, 1141–1145.

8 (a) Kumar, S.; Doshi, H.; Srinivasarao, M.; Park, J.-O.; Schiraldi, D. A. Polymer 2002, 43, 1701–1703; (b) Zeng, J.; Saltysiak, B.; Johnson, W. S.; Schiraldi, D. A.; Kumar, S. Compos B 2004, 35, 245–249; (c) Ma, H.; Zeng, J.; Realff, M. L.; Kumar, S.; Schiraldi, D. A. Compos Sci Technol 2003, 63, 1617–1628; (d) Sandler, J.; Windle, A. H.; Werner, P.; Altstädt, V.; Es, M. V.; Shaffer, M. S. P. J Mater Sci 2003, 38, 2135–2141; (e) Uchida, T.; Dang, T.; Min, B. G.; Zhang, X.; Kumar, S. Compos B 2005, 36, 183–187; (f) Kumar, S.; Dang, T. D.; Arnold, F. E.; Bhattacharyya, A. R.; Min, B. G.; Zhang, X.; Vaia, R. A.; Park, C.; Adams, W. W.; Hauge, R. H.; Smalley, R. E.; Ramesh, S.; Willis, P. A. Macromolecules 2002, 35, 9039–9043.

9 Song, Y.-S.; Youn, J.-R. Carbon 2005, 43, 1378–1385.

10 (a) Zhang, W. D.; Shen, L.; Phang, I. Y.; Liu, T. Macromolecules 2004, 37, 256–259; (b) Liu, T.; Phang, I. Y.; Shen, L.; Chow, S. Y.; Zhang, W. Macromolecules 2004, 37, 7214–7222; (c) Andrews, R.; Jacques, D.; Rao, A. M.; Rantell, T.; Derbyshire, F.; Chen, Y.; Chen, J.; Haddon, R. C. Appl Phys Lett 1999, 75, 1329–1331; (d) Qian, D.; Dickey, E. C.; Andrews, R.; Rantell, T. Appl Phys Lett 2000, 76, 2868–2870; (e) Shaffer, M. S. P.; Windle, A. H. Adv Mater 1999, 11, 937–941; (f) Jin, L.; Bower, C.; Zhou, O. Appl Phys Lett 1998, 73, 1197–1199; (g) Haggenmueller, R.; Gommans, H. H.; Rinzler, A. G.; Fischer, J. E.; Winey, K. I. Chem Phys Lett 2000, 330, 219–225; (h) Chen, G. Z.; Shaffer, M. S. P.; Coleby, D.; Dixon, G.; Zhou, W.; Fray, D. I.; Windle, A. H. Adv Mater 2000, 12, 522–526; (i) Sandler, J.; Shaffer, M. S. P.; Prasse, T.; Bauhofer, W.; Schulte, K.; Windle, A. H. Polymer 1999, 40, 5967–5971; (j) Park, C.; Ounaies, Z.; Watson, K. A.; Crooks, R. E.; Smith, J., Jr.; Lowther, S. E.; Connell, J. W.; Siochi, E. J.; Harrison, J. S.; St Clair, T. L. Chem Phys Lett 2002, 364, 303–308.

11 (a) Sun, Y.-P.; Fu, K.; Lin, Y.; Huang, W. Acc Chem Res 2002, 35, 1096–1104; (b) Dai, L.; Mau, W. H. Adv Mater 2001, 13, 899–913; (c) Hirsch, A. Angew Chem Int Ed 2002, 41, 1853–1859; (d) Banerjee, S.; Kahn, M. G. C.; Wong, S. S. Chem Eur J 2003, 9, 1898–1908; (e) Tasis, D.; Tagmatarchis, N.; Georgakilas, V.; Prato, M. Chem Eur J 2003, 9, 4000–4008; (f) Lin, Y.; Zhou, B.; Shiral Fernando, K. A.; Liu, P.; Allard, L. F.; Sun, Y.-P. Macromolecules 2003, 36, 7199–7204; (g) Mitchell, C. A.; Bahr, J. L.; Arepalli, S.; Tour, J. M.; Krishnamoorti, R. Macromolecules 2002, 35, 8825–8830.

12 (a) Zhang, T.; Shi, Z.; Gu, Z.; Iljima, S. Carbon 2000, 38, 2055–2059; (b) Huang, W.; Lin, Y.; Taylor, S.; Gaillard, J.; Rao, A. M.; Sun, Y.-P. Nano Lett 2002, 2, 231–234.

13 Heller, D. A.; Barone, P. W.; Strano, M. S. Carbon 2005, 43, 651–653.

14 (a) Hummers, W. S.; Offeman, R. E. J Am Chem Soc 1958, 80, 1339–1339; (b) Hu, H.; Zhao, B.; Itkis, M. E.; Haddon, R. C. J Phys Chem B 2003, 107, 13838–13842.

15 (a) Wei, C. Phys Lett 2006, 88, 93108–93110; (b) Wong, M.; Paramsothy, M.; Xu, X. J.; Ren, Y.; Li, S.; Liao, K. Polymer 2003, 44, 7757–7764; (c) Barber, A. H.; Cohen, S. R.; Eitan, A.; Schadler, L. S.; Wagner, H. D. Adv Mater 2006, 18, 83–87.

16 Tran, M. Q.; Cabral, J. T.; Shaffer, M. S. P.; Bismarck, A. Nano Lett 2008, 8, 2744–2750.

17 (a) Oh, S.-J.; Lee, H.-J.; Keum, D.-K.; Lee, S.-W.; Park, S.-Y.; Tan, L.-S.; Baek, J.-B. Polymer 2006, 47, 1132–1140; (b) Jeong, W.; Kessler, M. R. Chem Mater 2008, 20, 7760–7068.

18 Saeed, K.; Park, S.-Y.; Haider, S.; Baek, J.-B. Nanoscale Res Lett 2009, 4, 39–46.

19 (a) Baek, J.-B.; Lyons, C. B.; Tan, L.-S. J Mater Chem 2004, 14, 2052–2056; (b) Han, S.-W.; Oh, S.-J.; Tan, L.-S.; Baek, J.-B. Carbon 2008, 46, 1841–1849; (c) Lee, H.-J.; Han, S.-W.; Kwon, Y.-D.; Tan, L.-S.; Baek, J.-B. Carbon 2008, 46, 1850–1859.

20 (a) Wolfe, J. E. In Encyclopedia of Polymer Science and Technology, 2nd ed.; Mark, H. F.; Kroschmitz, J. I., Eds.; Wiley-Interscience: New York, 1988; Vol. 11, pp 602–635, and references are there in; (b) Adams, W. W.; Eby, R. K.; McLemore, D. E. Mater Res Soc Symp Proc 1989, 134, 351–359.

21 Eo, S.-M.; Oh, S.-J.; Tan, L.-S.; Baek, J.-B. Eur Polym Mater 2008, 44, 1603–1612.

22 (a) Cassidy, P. E. Thermally Stable Polymer; Marcel Dekker: New York, 1980; p 168; (b) Dawans, F.; Marvel, C. S. J Polym Sci Part A: Gen Pap 1965, 3, 3549–3571; (c) Brock, T.; Sherrington, D. C. Polymer 1992, 33, 1773–1777; (d) Arnold, F. E.; Van Deusen, R. L. Macromolecules 1969, 2, 497–502; (e) Milford, G. N., Jr. U.S. Patent 4,394,500, 1981; (f) Milford, G. N., Jr. U.S. Patent 4,460,763, 1984; (g) Chung, T. S. In Handbook of Thermoplastics; Olabisi, O., Ed., Marcel Dekker: New York, 1997; p 701.

23 (a) Afshari, M.; Sikkema, D. J.; Lee, K.; Bogle, M. Polym Rev 2008, 48, 230–274; (b) Chae, H. G.; Kumar, S. J. Appl Polym Sci 2006, 100, 791–802.

24 (a) Wainright, J. S.; Litt, M. H.; Savinell, R. F. In Handbook of Fuel Cells; Vielstich, W.; Lamm, A.; Gasteiger, H. A., Eds.; Wiley: New York, New York, 2003; Vol. 3, pp 436–446; (b) Asensio, J. A.; Borrós, S.; Gómez-Romero, P. J Electrochem Soc 2003, 151, A304–A310; (c) Asensio, J. A.; Borrós, S.; Gómez-Romero, P. Electrochem Commun 2003, 5, 967–972.

25 Asensio, J. A.; Gómez-Romero, P. Fuel Cells 2005, 5, 336–343.

26 Imai, Y.; Uno, K.; Iwakura, Y. Makromol Chem 1965, 83, 179–187.

27 Asensio, J. A.; Borrós, S.; Gómez-Romero, P. J Polym Sci Part A: Polym Chem 2002, 40, 3703–3710.

28 Litt, M.; Ameri, R.; Wang, Y.; Savinell, R.; Wainwright, J. Mater Res Soc Symp Proc 1999, 548, 313–323.

29 Kim, H.-J.; Cho, S. Y.; An, S. J.; Eun, Y. C.; Kim, J.-Y.; Yoon, H.-K.; Kweon, H.-J.; Yew, K. H. Macromol Rapid Commun 2004, 25, 894–897.

30 Strano, M. S.; Huffman, C. B.; Moore, V. C.; O'Connell, M. J.; Haroz, E. H.; Hubbard, J.; Miller, M.; Rialon, K.; Kittrell, C.; Ramesh, S.; Hauge, R. H.; Smalley, R. E. J Phys Chem B 2003, 107, 6979–6985.

31 Cheng, J.; Zhang, X.; Luo, Z.; Liu, F.; Ye, Y.; Yin, W.; Liu, W.; Han, Y. Mater Chem Phys 2006, 95, 3290–3301.

32 Itkis, M. E.; Peres, D.; Hung, R.; Niyogi, S.; Haddon, R. C. J Am Chem Soc 2005, 127, 3439–3448.

33 Wereta, A., Jr.; Gehatia, M. T. Polym Eng Sci 1978, 18, 204–209.

34 Asensio, J. A.; Borrós, S.; Gómez-Romero, P. J Membr Sci 2004, 241, 89–93.

35 Kim, T.-H.; Lim, T.-W.; Lee, J.-C. J Power Source 2007, 172, 172–179.

36 Vollrath, F.; Knight, D. P. Nature 2001, 410, 541–548.

37 (a) Kreuer, K. D. J Membr Sci 2001, 185, 29–39; (b) Pathapati, P. R.; Xue, X.; Tang, J. Renewable Energy 2004, 30, 1–22; (c) Ryder, A. G.; Power, S.; Glynn, T. J Appl Spectrosc 2003, 57, 73–79.

38 Catalan, J.; Claramunt, R. M.; Elguero, J.; Laynez, J.; Menendez, M.; Anvia, F.; Quian, J. H.; Taagepera, M.; Taft, R. W. J Am Chem Soc 1988, 110, 4105–4111.

39 At this stage, ABPBI/MWCNT composite is not suitable for fuel cell membrane application because of its high electrical conductivity that may cause electrical shorts.

40 http://www.hanhwananotech.co.kr.